6130 *Inorg. Chem.* **2009**, *48*, 6130–6141
DOI: 10.1021/ic900491r

Inorganic Chemistry
Article

Thermal- and Light-Induced Spin Crossover in Novel 2D Fe(II) Metalorganic Frameworks $\{Fe(4\text{-}PhPy)_2[M^{II}(CN)_x]_y\}\cdot sH_2O$: Spectroscopic, Structural, and Magnetic Studies

M. Seredyuk,[†] A. B. Gaspar,*[,‡] V. Ksenofontov,[†] M. Verdaguer,[§] F. Villain,[§] and P. Gütlich*[,†]

[†]*Institut fur Anorganische und Analytische Chemie, Johannes-Gutenberg-Universität, Staudinger-Weg 9, D-55099 Mainz, Germany,* [‡]*Institut de Ciència Molecular (ICMOL)/Departament de Química Inorgànica, Universitat de València, Edifici de Instituts de Paterna, Apartat de Correus 22085, 46071 València, Spain, and* [§]*Institut Parisien de Chimie Moléculaire, UMR CNRS 7201, FR-CNRS 2769, Université Pierre et Marie Curie, 4 place Jussieu, case courrier 42, 75252 Paris Cedex 05, France*

Received March 12, 2009

Five novel two-dimensional coordination polymers $\{Fe(4PhPy)_2[M^{II}(CN)_4]\}\cdot sH_2O$ (4PhyPy = 4-phenylpyridine; **1**: M^{II} = Pd, $s = 0$; **2**: M^{II} = Ni, $s = 0$; **3**: M^{II} = Pt, $s = 1$) and $\{Fe(4PhPy)_2[M^{I}(CN)_2]_2\}\cdot sH_2O$ (**4**: M^{I} = Ag, $s = 1$; **5**: M^{I} = Au, $s = 0.5$) exhibiting spin-crossover properties have been synthesized. They were characterized at various temperatures using X-ray absorption spectroscopy (XAS), powder X-ray diffraction (PXRD), differential scanning calorimetry (DSC), and magnetic susceptibility measurements. The occurrence of a cooperative thermal spin transition detected by the magnetic method is located at critical temperatures $T_c^{\downarrow}/T_c^{\uparrow}$ = 163 K/203 K (**1**), 135 K/158 K (**2**), and 172 K/221 K (**3**), and a less cooperative one is located at T_c = 188 K (**4**) and 225 K (**5**). Compounds **1**−**5** show an abrupt color change from yellow (high-spin (HS) state) to red (low-spin (LS) state) upon spin-state conversion. The dehydration of the compounds changes the type of the spin transition, making it more abrupt and shifting the critical temperature to higher temperatures. For **1** and **2**, XAS provides local structural information on the contraction of the FeN_6 coordination sphere upon the HS-to-LS transition, in line with the magnetic results. Variable-temperature characterization of **1** by X-ray diffraction evidences the very abrupt phase transition with a large hysteresis. A light-induced spin conversion (LIESST effect) is detected by magnetic measurements in **1**−**5** below 70 K.

Introduction

The construction of coordination compounds displaying physical and chemical properties ranging from magnetism or optical properties to their use in functions such as sorption−desorption, exchange, separation, and catalysis is an important topic in current chemistry.[1−9] A particular aspect of this research line concerns the combination of different properties in the same material to achieve interplay between them. Future technological demands will require multifunctional materials where several properties of a different physical or chemical nature are met in a single material.

Incorporation of spin-crossover (SCO) building blocks in multifunctional systems is particularly suitable for these purposes, as the labile electronic configuration of the iron units may be switched between the high-spin (HS) and low-spin (LS) states induced by a change of temperature, pressure, irradiation, or phase transition.[10−15] The spin transition may occur in a narrow temperature range for cooperative transitions; furthermore, hysteresis accompanies a first-order spin

*To whom correspondence should be addressed. E-mail: ana.b.gaspar@uv.es (A.B.G.), guetlich@uni-mainz.de (P.G.).

(1) Bureekaew, S.; Shimomura, S.; Kitagawa, S. *Sci. Technol. Adv. Mater.* **2008**, 014108.
(2) Tanaka, D.; Kitagawa, S. *Chem. Mater.* **2008**, *20*, 922–931.
(3) Lehn, J.-M. *Supramolecular Chemistry. Concepts and Perspectives*; VCH: Weinheim, Germany, 1995.
(4) Kitagawa, S.; Kitaura, R.; Noro, S.-i. *Angew. Chem., Int. Ed. Engl.* **2004**, *43*, 2334–2375.
(5) Eddaoudi, M.; Kim, J.; Rosi, N.; Vodak, D.; Wachter, J.; O'Keeffe, M.; Yaghi, O. M. *Science* **2002**, *295*, 469–472.
(6) Yaghi, O. M.; O'Keeffe, M.; Ockwig, N. W.; Chae, H. K.; Eddaoudi, M.; Kim, J. *Nature* **2003**, *423*, 705–714.
(7) Rosseinsky, M. J. *Microporous Mesoporous Mater.* **2004**, *73*, 15–30.
(8) Férey, G.; Mellot-Draznieks, C.; Serre, C.; Millange, F.; Dutour, J.; Surblé, S.; Margiolaki, I. *Science* **2005**, *309*, 2040–2042.
(9) Matsuda, R.; Kitaura, R.; Kitagawa, S.; Kubota, Y.; Belosludov, R. V.; Kobayashi, T. C.; Sakamoto, H.; Chiba, T.; Takata, M.; Kawazoe, Y.; Mita, Y. *Nature* **2005**, *436*, 238–241.
(10) Gütlich, P.; Hauser, A.; Spiering, H. *Angew. Chem., Int. Ed. Engl.* **1994**, *33*, 2024–2054.
(11) Gütlich, P.; Goodwin, H. A. *Top. Curr. Chem.* **2004**, *233*, 1–47.
(12) Real, J. A.; Gaspar, A. B.; Muñoz, M. C. *Dalton Trans.* **2005**, 2062–2079.
(13) Murray, K. S. *Eur. J. Inorg. Chem.* **2008**, 3101–3121.
(14) Real, J. A.; Andres, E.; Muñoz, M. C.; Julve, M.; Granier, T.; Bousseksou, A.; Varret, F. *Science* **1995**, *268*, 265–267.
(15) Halder, G. J.; Kepert, C. J.; Moubaraki, B.; Murray, K. S.; Cashion, J. D. *Science* **2002**, *298*, 1762–1765.

 Published on Web 05/22/2009

transition when the structural changes are transmitted cooperatively throughout the whole solid.

In recent years, iron(II)-based cyanidometalate coordination polymers were the subject of research in several groups,[16−40] which particularly led to the detailed investigation of 1−3D SCO coordination polymeric networks of the type $\{Fe(L)_n[M^{II}(CN)_4]\}\cdot sH_2O$ or $\{Fe(L)_n[M^{I}(CN)_2]_2\}\cdot sH_2O$ (L = monodentate or bidentate polypyridyl ligand; n = 1, 2; M^{II} = Ni, Pd, Pt; M^{I} = Cu, Ag, Au; $s \geq 0$). Such compounds not only display interesting pressure- and light-induced properties but also can combine their cooperative spin-transition properties (magnetic, chromatic, and structural) with different chemical properties such as metallophilicity or crystalline-state ligand-substitution reactions with remarkable structural changes. Many of them show abrupt complete SCO near room temperature with a thermal hysteresis. This together with the recently reported complete HS ↔ LS switch of {Fe(pyrazine)[Pt(CN)$_4$]} through the use of a laser pulse inside the hysteresis loop centered at room temperature[29,35] makes these kinds of materials attractive for current scientific and technological research.

The SCO phenomenon has recently been investigated in the framework of other materials of technological interest such as liquid crystals.[41−43] A single material combining spin-crossover and liquid-crystalline behavior may lead to a number of advantages in practical applications, for example, processing spin-crossover materials in the form of thin films, enhancement of spin-transition signals, switching and sensing in different temperature regimes, or achievement of photo- and thermochromism in Fe(II)-containing liquid crystals. The change of color is certainly a phenomenon which is of interest in the field of liquid crystals. The interest lies in the necessity of a color change in a number of applications in liquid crystals such as passive blocking filters, laser addressed devices, polarizers based on dichroic effects, or the utility of thermochromism.

It has recently been shown that synchronization of spin-state and liquid-crystal transitions in Fe(II) metallomesogens is achieved by the search for a parent SCO system suitable, after attaching the liquid crystal moiety, of possessing a LS state or SCO properties at the temperature where the solid−liquid crystal transition is foreseen (275−400 K). Although few examples of Fe(II) metallomesogens have been reported, a very rich interplay or synergy between spin-transition and liquid-crystal phase transition has been observed in the following: (i) systems with coupled phase transitions, subdivided into three groups *a*, *b*, and *c* (in *a*, the structural changes associated with the Cr ↔ LC drive the spin transition, while in *b*, these structural changes influence the spin state of the metallic centers but are not the driving force of the spin state transition; c concerns the systems where the vitrification of the material inhibits the SCO properties),[41−45] (ii) systems where both transitions coexist in the same temperature region but are not coupled due to competition with the dehydration,[41,43,45,46] and (iii) systems with uncoupled phase transitions.[47]

Up to now, the investigations have been centered in mononuclear and one-dimensional Fe(II) metallomesogens based on tripodand Schiff bases formed by symmetrical triamines and heterocyclic aldehydes and substituted triazole ligands that incorporate long alkyl chains. In this regard, we presently aim to explore the possibility of achieving similar physical properties by modifying chemically two-dimensional cyanide-bridged Fe(II) SCO polymers.

From the chemical point of view, the layered organization of the iron(II) two-dimensional cyanidometalate coordination polymers with monodentate ligands (e.g., with pyridine and its derivatives) might be well suited for grafting the liquid

(16) Kitazawa, T.; Gomi, Y.; Takahashi, M.; Takeda, M.; Enomoto, M.; Miyazaki, A.; Enoki, T. *J. Mater. Chem.* **1996**, *6*, 119–121.
(17) Sato, T.; Ambe, F.; Kitazawa, T.; Sano, H.; Takeda, M. *Chem. Lett.* **1997**, *12*, 1287–1288.
(18) Kitazawa, T.; Takahashi, M.; Takahashi, M.; Enomoto, M.; Miyazaki, A.; Enoki, T.; Takeda, M. *J. Radioanal. Nucl. Chem.* **1999**, *239*, 285–290.
(19) Kitazawa, T.; Eguchi, M.; Takeda, M. *Mol. Cryst. Liq. Cryst.* **2000**, *341*, 1331–1336.
(20) Niel, V.; Martinez-Agudo, J. M.; Muñoz, M. C.; Gaspar, A. B.; Real, J. A. *Inorg. Chem.* **2001**, *40*, 3838–3839.
(21) Niel, V.; Muñoz, M. C.; Gaspar, A. B.; Galet, A.; Levchenko, G.; Real, J. A. *Chem.—Eur. J.* **2002**, *8*, 2446–2453.
(22) Galet, A.; Niel, V.; Muñoz, M. C.; Real, J. A. *J. Am. Chem. Soc.* **2003**, *125*, 14224–14225.
(23) Hosoya, K.; Kitazawa, T.; Takahashi, M.; Takeda, M.; Meunier, J. F.; Molnar, G.; Bousseksou, A. *Phys. Chem. Chem. Phys.* **2003**, *5*, 1682–1688.
(24) Kitazawa, T.; Hosoya, K.; Takahashi, M.; Takeda, M.; Marchuk, I.; Filipek, S. M. *J. Radioanal. Nucl. Chem.* **2003**, *255*, 509–512.
(25) Molnar, G.; Niel, V.; Real, J. A.; Dubrovinsky, L.; Bousseksou, A.; McGarvey, J. J. *J. Phys. Chem. B* **2003**, *107*, 3149–3155.
(26) Niel, V.; Galet, A.; Gaspar, A. B.; Muñoz, M. C.; Real, J. A. *Chem. Commun.* **2003**, 1248–1249.
(27) Niel, V.; Thompson, A. L.; Muñoz, M. C.; Galet, A.; Goeta, A. S. E.; Real, J. A. *Angew. Chem., Int. Ed. Engl.* **2003**, *42*, 3760–3763.
(28) Garcia, Y.; Niel, V.; Muñoz, M. C.; Real, J. A. *Top. Curr. Chem.* **2004**, *233*, 229–257.
(29) Bonhommeau, S.; Molnar, G.; Galet, A.; Zwick, A.; Real, J. A.; McGarvey, J. J.; Bousseksou, A. *Angew. Chem., Int. Ed. Engl.* **2005**, *44*, 4069–4073.
(30) Molnar, G.; Guillon, T.; Moussa, N. O.; Rechignat, L.; Kitazawa, T.; Nardone, M.; Bousseksou, A. *Chem. Phys. Lett.* **2006**, *423*, 152–156.
(31) Munoz, M. C.; Gaspar, A. B.; Galet, A.; Real, J. A. *Inorg. Chem.* **2007**, *46*, 8182–8192.
(32) Rodríguez-Velamázan, J. A.; Castro, M.; Palacios, E.; Burriel, R.; Kitazawa, T.; Kawasaki, T. *J. Phys. Chem. B* **2007**, *111*, 1256–1261.
(33) Agustí, G.; Cobo, S.; Gaspar, A. B.; Molnar, G.; Moussa, N. O.; Szilagyi, P. A.; Palfi, V.; Vieu, C.; Muñoz, M. C.; Real, J. A.; Bousseksou, A. *Chem. Mater.* **2008**, *20*, 6721–6732.
(34) Agustí, G.; Muñoz, M. C.; Gaspar, A. B.; Real, J. A. *Inorg. Chem.* **2008**, *47*, 2552–2561.
(35) Cobo, S.; Ostrovskii, D.; Bonhommeau, S.; Vendier, L.; Molnar, G.; Salmon, L.; Tanaka, K.; Bousseksou, A. *J. Am. Chem. Soc.* **2008**, *130*, 9019–9024.
(36) Kosone, T.; Kachi-Terajima, C.; Kanadani, C.; Saito, T.; Kitazawa, T. *Chem. Lett.* **2008**, *37*, 754–755.
(37) Kosone, T.; Kachi-Terajima, C.; Kanadani, C.; Saito, T.; Kitazawa, T. *Chem. Lett.* **2008**, *37*, 422–423.
(38) Nakao, K.; Hayami, S.; Akita, M.; Inoue, K. *Chem. Lett.* **2008**, *37*, 292–293.
(39) Kosaka, W.; Nomura, K.; Hashimoto, K.; Ohkoshi, S.-i. *J. Am. Chem. Soc.* **2005**, *127*, 8590–8591.
(40) Arai, M.; Kosaka, W.; Matsuda, T.; Ohkoshi, S.-i. *Angew. Chem., Int. Ed. Engl.* **2008**, *47*, 6885–6887.
(41) Seredyuk, M.; Gaspar, A. B.; Ksenofontov, V.; Reiman, S.; Galyametdinov, Y.; Haase, W.; Rentschler, E.; Gütlich, P. *Chem. Mater.* **2006**, *18*, 2513–2519.
(42) Seredyuk, M.; Gaspar, A. B.; Ksenofontov, V.; Galyametdinov, Y.; Kusz, J.; Gütlich, P. *Adv. Funct. Mater.* **2008**, *18*, 2089–2101.
(43) Seredyuk, M.; Gaspar, A. B.; Ksenofontov, V.; Galyametdinov, Y.; Kusz, J.; Gütlich, P. *J. Am. Chem. Soc.* **2008**, *130*, 1431–1439.
(44) Seredyuk, M.; Gaspar, A. B.; Ksenofontov, V.; Galyametdinov, Y.; Verdaguer, M.; Villain, F.; Gütlich, P. *Inorg. Chem.* **2008**, *47*, 10232–10245.
(45) Seredyuk, M.; Gaspar, A. B.; Ksenofontov, V.; Reiman, S.; Galyametdinov, Y.; Haase, W.; Rentschler, E.; Gütlich, P. *Hyperfine Interact.* **2006**, *166*, 385–390.
(46) Fujigaya, T.; Jiang, D. L.; Aida, T. *J. Am. Chem. Soc.* **2003**, *125*, 14690–14691.
(47) Gaspar, A. B.; Seredyuk, M.; Gütlich, P. *Coord. Chem. Rev.* **2008**, doi: 10.1016/j.ccr.2008.11.016.

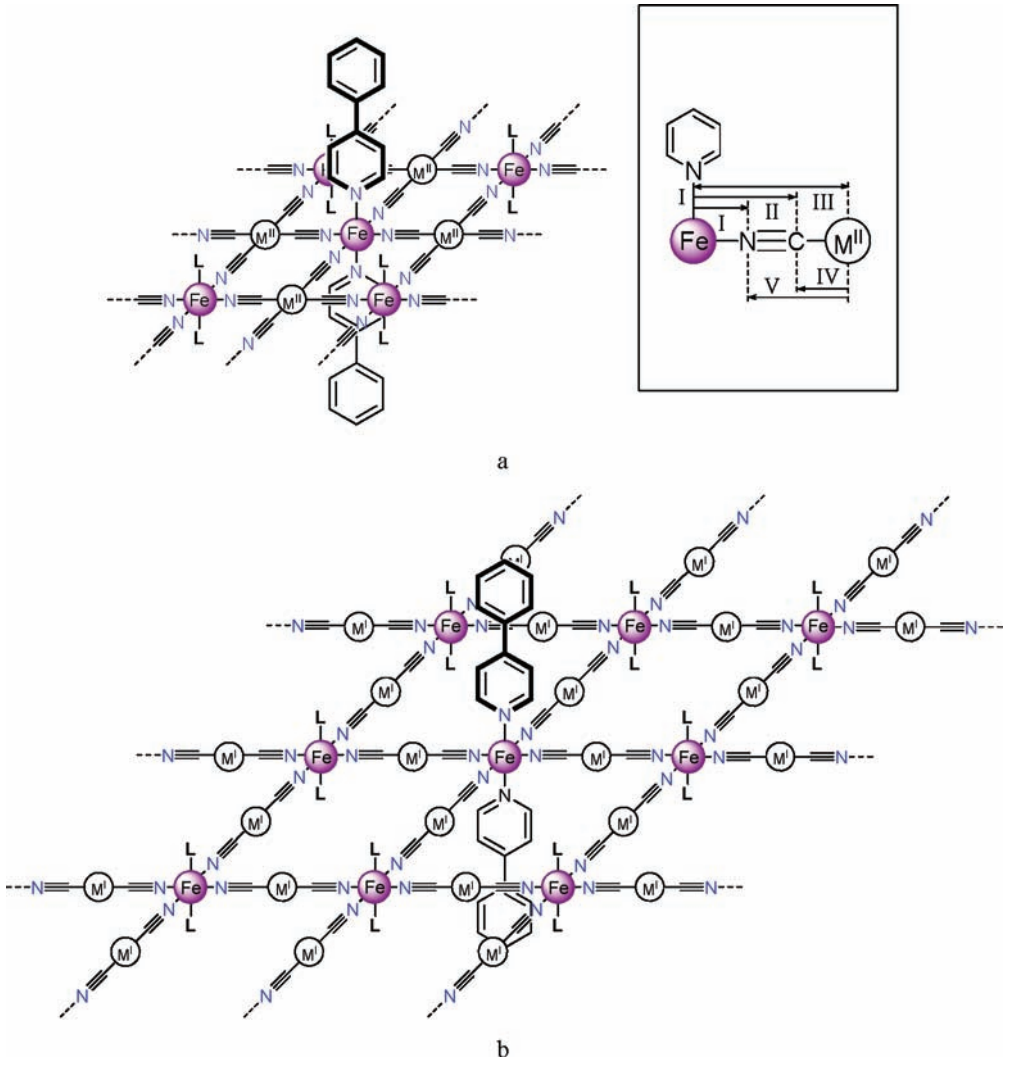

Figure 1. Schematic structures of (a) **1**, **2**, and **3** (M^{II} = Pd, Ni, and Pt, respectively) and (b) of **4** and **5** (linear M^{I} = Ag and Au, respectively). For simplicity, the structural formula of the ligand 4-phenylpyridine is shown for the central iron ions only; for the rest, it is shortened to L. The inset shows scattering pathways at the iron *K*-edge (I, II, III) and nickel *K*-edge (IV, V, III) observable in the EXAFS Fourier transforms.

crystal chemical functionality without substantial perturbation of the polymeric arrays. The first step in this study, obviously, is the investigation of the unsubstituted "parent" SCO compound lacking any additional substituents. In this regard, we report here a new family of two-dimensional SCO coordination polymers based on bridging metalocyanides $[M^{II}(CN)_4]^{2-}$ and $[M^{I}(CN)_2]^{-}$ and ligand 4-phenylpyridine (4PhPy). In particular, the synthesis and spectroscopic and physical characterization of $\{Fe(4PhPy)_2[M^{II}(CN)_4]\}\cdot sH_2O$ (**1**: M^{II} = Pd, s = 0; **2**: M^{II} = Ni, s = 0; **3**: M^{II} = Pt, s = 1) and $\{Fe(4PhPy)_2[M^{I}(CN)_2]_2\}\cdot sH_2O$ (**4**: M^{I} = Ag, s = 1; **5**: M^{I} = Au, s = 0.5) will be discussed in detail.

Results

X-Ray Absorption Spectroscopy (XAS) Structural Characterization of 1 and 2. In the family of Hofmann-like polymers of iron(II) with monodentate ligands, the X-ray single-crystal structure is known for $\{Fe(py)_2[Ni(CN)_4]\}$ and related compounds.[16,19] The fragment of the 2D polymeric structure sketched in Figure 1a consists of iron(II) ions surrounded by pyridine moieties and bridging tetracyanidonickelate anions. All attempts performed in order to obtain single crystals of compounds **1**−**3** suitable for X-ray diffraction were unsuccessful. Therefore, we have used extended X-ray absorption fine structure (EXAFS) spectroscopy for their structural characterization. This technique provides the possibility of evaluating the local environment of the metal using powder samples and, additionally, measurements at different temperatures at the iron *K*-edge which allows a following of the changes in the Fe coordination sphere, in particular the Fe−N distances.

Figure 2 shows the normalized edge spectra of complexes **1** and **2** at different temperatures. In both complexes, the energy of the *K*-edge is shifted to lower energy, demonstrating (at a constant oxidation state) the increased Fe−N distances associated with the HS−LS spin transition. In the heating and cooling runs, the variation of the energies of the edge follows the magnetic behavior discussed below (Figure 3). The radial distributions for **1** and **2** at low and high temperatures are presented in Figure 4. In the Fourier transform spectra, each atomic shell surrounding the iron is represented by a peak (see inset in Figure 1a). The first shell (I) is formed by nitrogen atoms which belong to bridging tetracyanide groups in the equatorial plane and to axial pyridine molecules.

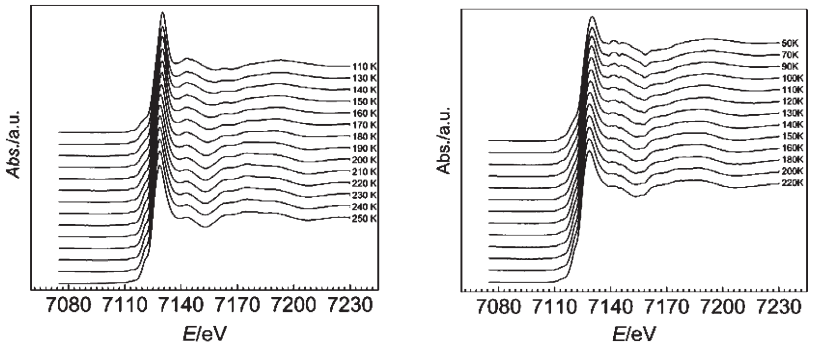

Figure 2. Iron *K*-edge spectra of complexes **1** (a) and **2** (b) at different temperatures.

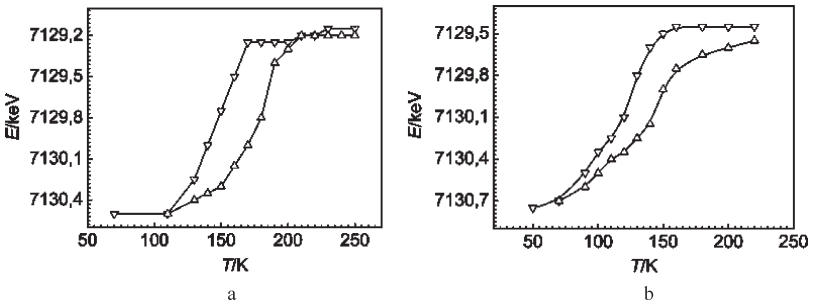

Figure 3. Variation of iron *K*-edge energy of **1** (a) and **2** (b) in the subsequent cooling and heating runs.

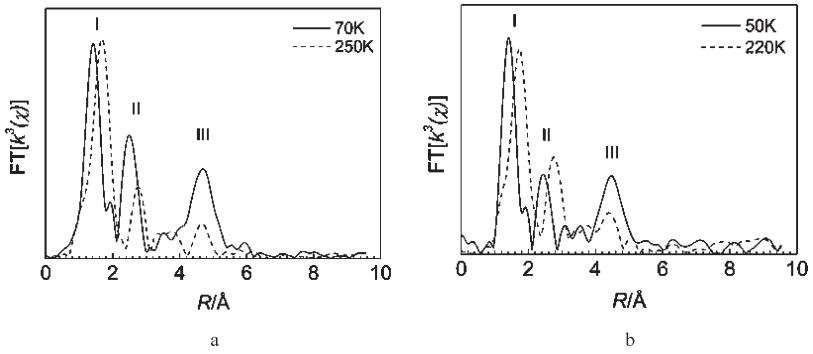

Figure 4. Fourier transforms of iron *K*-edge EXAFS signal for **1** (a) and **2** (b) at low and high temperatures. I, II, and III correspond to Fe−N, Fe−C, and Fe−M (M = Pd or Ni) distances, respectively.

The second one (II) includes carbon atoms of cyanido groups and of pyridine cycles. The third shell (III) is essentially due to heavy Pd/Ni atoms of the $[Pd(CN)_4]$/$[Ni(CN)_4]$ groups. Assigning of the peaks can also be supported by the form of filtered signals, which is exponential for light atoms like N and C and nonexponential for heavier Pd/Ni atoms (see the Supporting Information, SFigure 1). For shells II and III, multiple scattering complicates a simple evaluation of the structural parameters; therefore, for these two, only qualitative evaluation is reported here. Using a simple scattering model, we could analyze quantitatively the first shell of neighbors I, which reflects the structural transformation accompanying the spin transition (see the Supporting Information, STable 1). The relevant structural EXAFS data along with the single-crystal X-ray data of spin-crossover iron(II) cyanide bridged polymers related to compounds **1**−**3** are grouped in Table 1. The fitted bond distances for the first FeN_6 coordination shell compare well with that of related iron(II) polymers in both spin states. The transition curves derived from the EXAFS data resemble the magnetic ones (Figure 5a,b).

For **2**, XAS was used at the iron *K*-edge at different temperatures and at the nickel *K*-edge at 250 K. Both sets of data show similar patterns with three dominant peaks attributed to the first three coordination shells (Figure 6). It is worth to stress the fact that peak III at the iron *K*-edge is rather intense and almost disappears at the nickel *K*-edge. Additionally, the second peak II at the iron *K*-edge is much less intense than the one at the nickel *K*-edge (V). We think that both features can be understood in the following scheme: the $Ni(CN)_4$ groups are slightly tilted, and the angle Fe−C−N deviates from 180° while the Ni−C−N angle is perfectly aligned, as observed in the analogous compound $\{Fe(py)_2[Ni(CN)_4]\}$.[16] This is the reason why at the nickel *K*-edge a focusing effect on N (large intensity of peak V) is observed and not on the Fe (Fe is almost invisible in the Fourier transform, Figure 6). On the other hand, at the iron *K*-edge the focusing effect on Ni through the carbon atom intensifies the signal of Ni

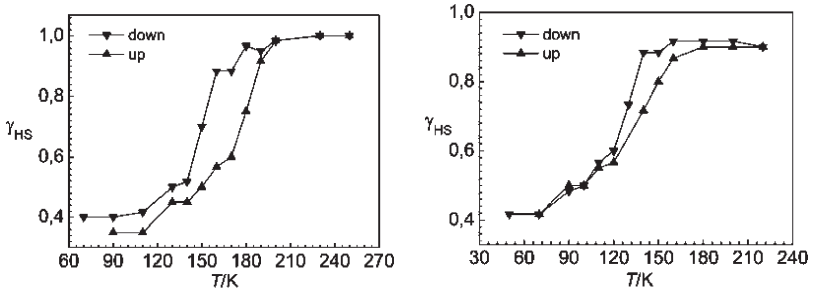

Figure 5. Thermal variation of the high-spin fraction γ_{HS} computed from the EXAFS data for **1** (a) and **2** (b).

Table 1. Relevant Structural Data of Iron(II) Hofmann Clathrates

compound	< Fe−N > /Å, LS	< Fe−N > /Å, HS	source
1	1.95	2.17	this work
2	1.94	2.16	this work
$\{Fe(pmd)_2[Cu(CN)_2]_2\}$ pmd = pyrimidine		2.17	26
$[Fe(pmd)(H_2O)\{Ag(CN)_2\}_2]\cdot H_2O$	1.95	2.17	27
$[Fe(pmd)(H_2O)\{Au(CN)_2\}_2]\cdot H_2O$	1.96	2.18	27
$\{Fe(py)_2[Ag(CN)_2]_2\}$ py = pyridine		2.21	32
$\{Fe(py)_2[Ni(CN)_4]\}$		2.24	16
$\{Fe(pz)[Ag(CN)_2]_2\}$ pz = pyrazine	1.93	2.17	21
$\{Fe(pz)[Pt(CN)_4]\}$		2.16	20
$\{Fe(3CNpy)_2[Ag(CN)_2]_2\}\cdot 2/3H_2O$ 3CNpy = 3-cyanopyridine	1.96	2.16	22
$\{[Fe(3\text{-}Fpy)_2][Au(CN)_2]_2\}$ 3-Fpy = 3-fluoropyridine		2.18	37
$\{Fe(4,4'\text{-bipy})_2[Ag(CN)_2]_2\}$ 4,4′-bipy = 4,4′-bipyridine		2.18	21
$\{Fe(bpe)_2[Ag(CN)_2]_2\}$ bpe = bispyridylethylene		2.18	21
$\{Fe(2\text{-}Mepy)_2[Ni(CN)_4]\}$ 2-MePy = 2-methylpyridine		2.20	19
$\{Fe(3\text{-}Mepy)_2[Ni(CN)_4]\}$ 3-MePy = 3-methylpyridine		2.16	19
$\{Fe(4\text{-}Mepy)_2[Ni(CN)_4]\}$ 4-MePy = 4-methylpyridine		2.17	19

in the Fourier transform but not on the C (peak II is much less intense than peak V). At the iron *K*-edge, **2** has the same first coordination shell as **1** (six nitrogen neighbors, Fe−N distance is 1.95 Å in LS state and 2.16 Å in HS state, the Supporting Information, STable 2) and the same second shell (carbon atoms of CN groups and pyridines). The third shell of the heavy neighbor (Ni) appears at about 4.8 Å. The significant intensity of the last peak is due to the focusing effect in linear cyanide bridges.[48] At the nickel *K*-edge, the peaks in the Fourier transform are assigned to four carbon atoms of cyanide ligands (mean distance = 1.88 Å) for the first shell, to the (cyanide) nitrogen atoms for the second shell, and to iron atoms for the third shell, visible at ca. 4.7 Å. The analysis of the Ni−C shell is given in STable 3 (the Supporting Information).

Powder X-Ray Diffraction (PXRD). The evolution of the diffraction patterns of **1** with the temperature in the form of contour plots is shown in Figure 7a,b. The data have been collected for values of the diffraction angle of $1° \leq 2\theta \leq 14°$ for increasing and decreasing temperatures. The LS state diffraction pattern (low temperature) significantly differs from the HS state diffraction pattern (high temperature). For the narrow range of intermediate temperatures, the diffraction pattern is a superposition of the two patterns for the pure ground states with temperature-dependent relative intensities. The observation demonstrates a crystallographic phase change at the same temperature as the spin transition. To better describe the phase transition, the intensity of the two well-resolved diffraction peaks at $2\theta = 1.50°$ for the HS state and

(48) Yokoyama, T.; Murakami, Y.; Kiguchi, M.; Komatsu, T.; Kojima, N. *Phys. Rev. B: Condens. Matter* **1998**, *58*, 14238–14244.

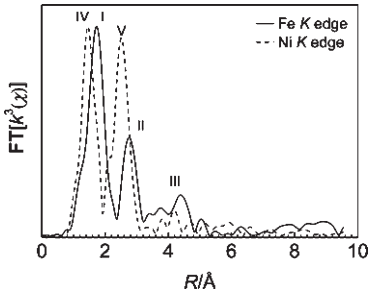

Figure 6. Comparison of Fourier transforms of the EXAFS spectra at Ni and Fe *K* edges of complex **2** at 250 and 220 K, respectively. Roman digits I−V correspond to the scattering pathways shown in Figure 1a (inset).

at $2\theta = 1.52°$ for the LS state has been evaluated by a least-squares fit to the Gaussian line shape. In Figure 7c, the intensity ratio I_{HS}/I_{total} is plotted as a function of the temperature for heating and cooling modes. The phase transition is complete at both extremes of the temperature range with $T_c^{\downarrow} = 151$ K and $T_c^{\uparrow} = 205$ K; the width of the hysteresis loop is 54 K, in good agreement with the magnetic data discussed below.

The PXRD patterns of compounds **2**−**5** are shown in SFigure 2a,b (the Supporting Information). The fact that the powder X-ray patterns of **2** and **3** are not similar to those of **1** does not rule out a similar structure for these complexes, as slightly different packing and lattice arrangements would yield different crystallographic patterns even for similar structures. In **4** and **5**, some regions of the diffraction patterns are similar, but it is impossible to conclude anything about the isomorphism of the two compounds. The structures of **4** and **5** are apparently

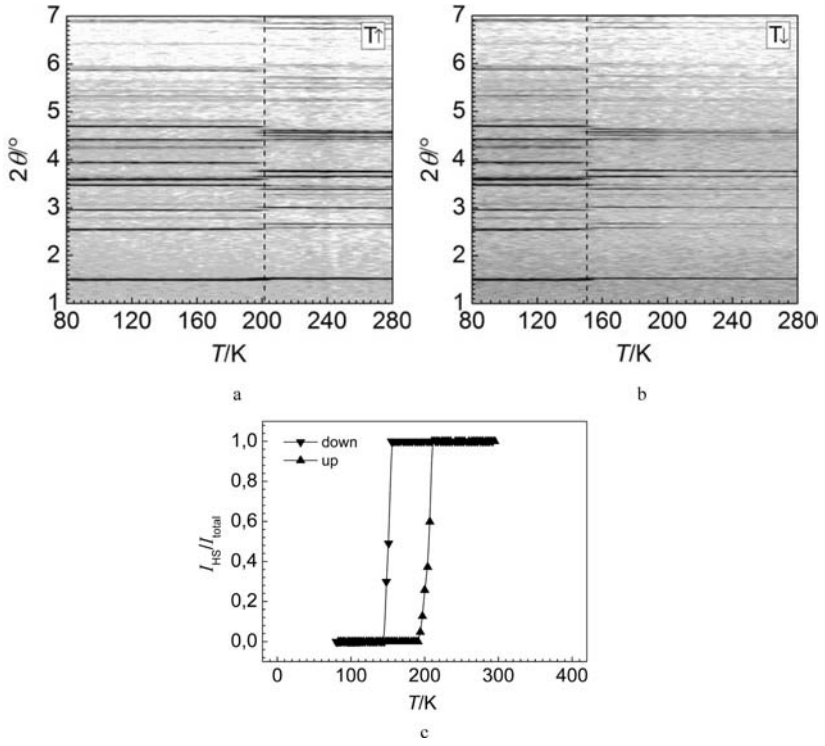

Figure 7. Contour plots showing the evolution of the diffraction pattern of **1** in heating (a) and cooling (b) modes which confirm the occurrence of the structural hysteresis. Darker means higher intensity. (c) Temperature dependence of the ratio I_{HS}/I_{total} for **1** based on two peaks at 1.50−1.52°.

similar to those reported for $\{Fe(py)_2[Ag(CN)_2]_2\}$,[32] $\{Fe(py)_2[Au(CN)_2]_2\}$[36] and related compounds.[34,37]

IR Spectroscopy and EDXA Data. The formation of M−C≡N−M′ bridges in the polynuclear complexes **1**−**5** is evidenced by the stretching vibrations of the cyanide ligands. Selected IR data are summarized in Table 2. The ν(CN) modes are shifted to higher frequencies compared to those of the terminal cyanides of $K[M^I(CN)_2]$ or $K_2[M^{II}(CN)_4]$ salts, confirming the formation of the polymeric heterometallic structures.[49,50]

Evidence that heterometallic networks are formed is also found by energy-dispersive X-ray microanalysis (EDXA) spectroscopy. A scan of powdered samples shows both Fe and M peaks, and the quantitative analysis of the integrated areas of the multiplex scans yields an Fe/M ratio of 1:1 ± 5% (M = Pd, Ni, or Pt) or 1:2 ± 5% (M = Ag or Au). The two ratios corresponds to the situations described in Figure 1a,b where the Fe^{2+} ions are incorporated into the face-centered square grid assemblies.

Magnetic Susceptibility Measurements. The thermal dependence of the product $\chi_M T$ (χ_M being the molar susceptibility and T the temperature) for compounds **1**−**5** is displayed in Figure 8. The temperature dependence of the magnetic susceptibility was recorded at a rate of 2 K min^{-1}.

The $\chi_M T$ value for all compounds at room temperature is near 3.50 cm^3 K mol^{-1}, which reveals the HS configuration. Upon cooling, the magnetic susceptibility of **1** diminishes abruptly, providing evidence of the HS ↔ LS transition. The warming run reveals the occurrence of a 40 K wide hysteresis loop with $T_c^{\downarrow}$ = 163 K and $T_c^{\uparrow}$ = 203 K. This feature is indicative of a strong cooperative first-order character of the transition. It is stronger than in $\{Fe(py)_2[Pd(CN)_4]\}$,[20] where the critical temperature is about the same ($< T_c > \approx$ 210 K) but the width of the hysteresis loop is smaller (5 K). A reasonable explanation for the observed behavior in **1** could be a larger interaction between spin-crossover centers through the phenyl moieties of the ligands.

Table 2. Infrared Data of **1**−**5**

	ν(CN)/cm^{-1}
$K[Ag(CN)_2]$[50]	2143
$K_2[Ni(CN)_4]$[50]	2130
1	2164
2	2152
3	2162
4	2176
5	2165

The hysteresis loop of **2** is asymmetric, as that of $\{Fe(py)_2[Ni(CN)_4]\}$.[20] However, it occurs at lower temperatures. The critical temperatures are $T_c^{\downarrow}$ = 135 K and $T_c^{\uparrow}$ = 158 K in the cooling and heating modes, respectively. In comparison with the hydrated compound **2**·H_2O reported by Nakao et al.,[38] the cooperativity of the dehydrated compound is strengthened, which is reflected by the increasing width of the loop and more complete HS ↔ LS conversion in the low-temperature region. Despite that, the transition is still incomplete, and a decrease of the susceptibility is observed below 30 K due to the zero-field splitting (ZFS) of the S = 2 state of the Fe(II) ions.[51]

(49) Zhan, S.-z.; Guo, D.; Zhang, X.-y.; Du, C.-x.; Zhu, Y.; Yang, R.-n. *Inorg. Chim. Acta* **2000**, *298*, 57–62.
(50) Nakamoto, K. *Infrared and Raman Spectra of Inorganic and Coordination Compounds*; John Wiley: New York, 1986.
(51) Carlin, L. R. *Magnetochemistry*; Springer: Berlin, 1986.

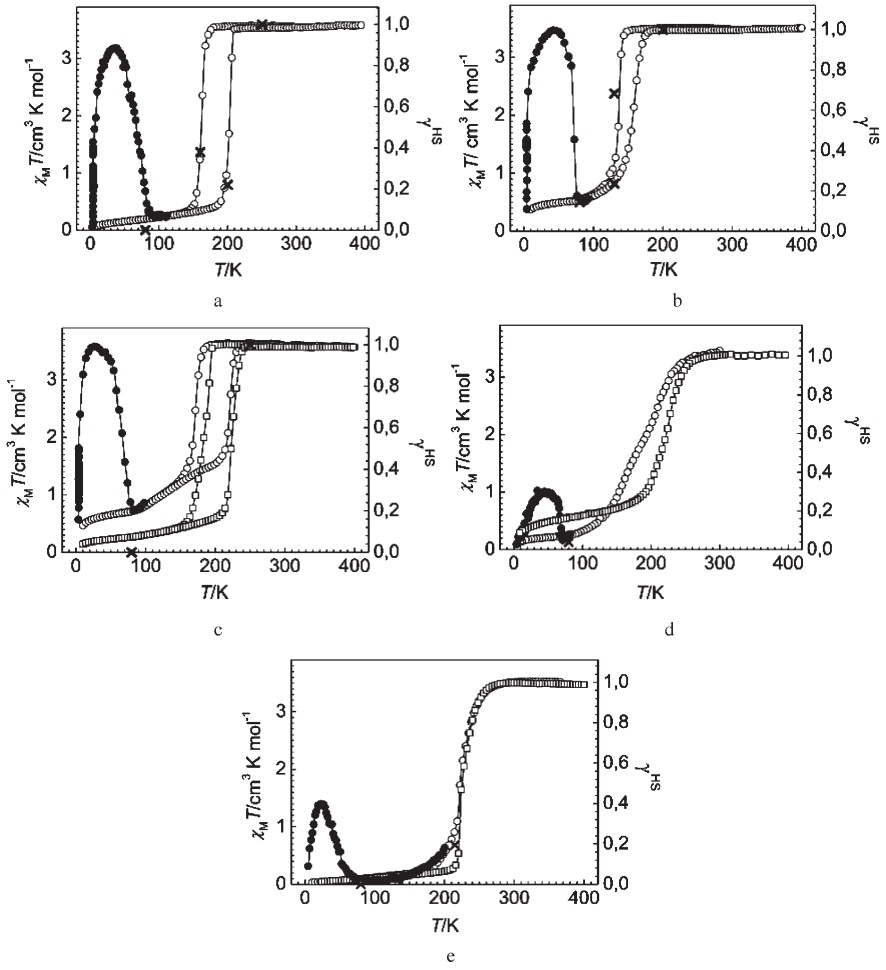

Figure 8. Thermal variation of the $\chi_M T$ product from magnetic measurements of the pristine (○) and dehydrated (□) forms of **1** (a), **2** (b), **3** (c), **4** (d), and **5** (e). LIESST effect (●) upon irradiation at 4 K with subsequent moving up in temperature and the γ_{HS} values derived from the Mössbauer data (×).

Contrary to compounds **1** and **2**, in the pristine form, compound **3** contains one molecule of water per monomeric unit, and this is reflected in the magnetic behavior of the compound. It is known that in iron(II) polymers solvent guest molecules strongly influence the spin-crossover behavior, shifting the temperature of the transition and changing the form of the transition curve.[27,29,33] Thus, despite the cooperative behavior being retained in pristine **3** with $T_c^{\uparrow}$ = 172 K and $T_c^{\downarrow}$ = 221 K, the transition is incomplete with a substantial HS fraction at low temperatures. If the compound is heated up to 400 K inside the SQUID magnetometer, dehydration occurs, and the magnetic behavior becomes very similar to that of **1** with parameters $T_c^{\downarrow}$ = 185 K and $T_c^{\uparrow}$ = 225 K.

Irradiation of the pristine compounds **1**−**3** at 4 K with a green laser (λ = 514 nm) caused quantitative photoconversion of the LS molecules into a metastable HS state. This LIESST effect[10,52] is shown in Figure 8a−c. The critical temperature of relaxation of the HS metastable state known as T^{LIESST} is 70, 72, and 66 K for **1**, **2**, and **3**, respectively.

The magnetic behavior of **4** is shown in Figure 8d. The pristine hydrated compound reveals a complete and continuous spin conversion which occurs in two poorly resolved steps, similarly to the pyridine analogue,[32] with $T_{1/2}(1)$ = 213 K and $T_{1/2}(2)$ = 162 K. As the temperature decreases, a constant value of $\chi_M T$ is maintained down to around 270 K, followed by a decrease to 2.00 cm^3 K mol^{-1} at 190 K. Further down to 70 K, the susceptibility shows a second smooth decrease, reaching finally a value of 0.10 cm^3 K mol^{-1}. Heating up to 400 K causes dehydration of the compound, as shown by the thermogravimetric analysis (TGA) data (see SFigure 3, Supporting Information), and modifies the magnetic properties. The dehydrated compound reveals quite an abrupt spin transition without hysteresis centered at 226 K. Similarly, the magnetic behavior of **5** is cooperative both in the pristine and hydrated form; however, dehydration leads to a sharpening of the low-temperature extremity of the transition curve. The critical temperature in both forms is equal to 225 K. The LIESST experiments in **4** and **5** have been performed on the pristine compounds. In both cases, the LS → HS conversion is incomplete, with T^{LIESST} = 71 and 44 K, respectively.

Mössbauer Spectroscopy Data. The temperature dependence of the ^{57}Fe Mössbauer spectra of **1**−**5** has been studied in low- and high-temperature regions. Figure 9 shows some representative spectra of **1** obtained in the heating and cooling modes. At 80 K, only a LS doublet is observed, at 250 K, only a HS one, whereas in the

(52) Létard, J. F.; Guionneau, P.; Nguyen, O.; Costa, J. S.; Marcen, S.; Chastanet, G.; Marchivie, M.; Goux-Capes, L. *Chem.—Eur. J.* **2005**, *11*, 4582–4589.

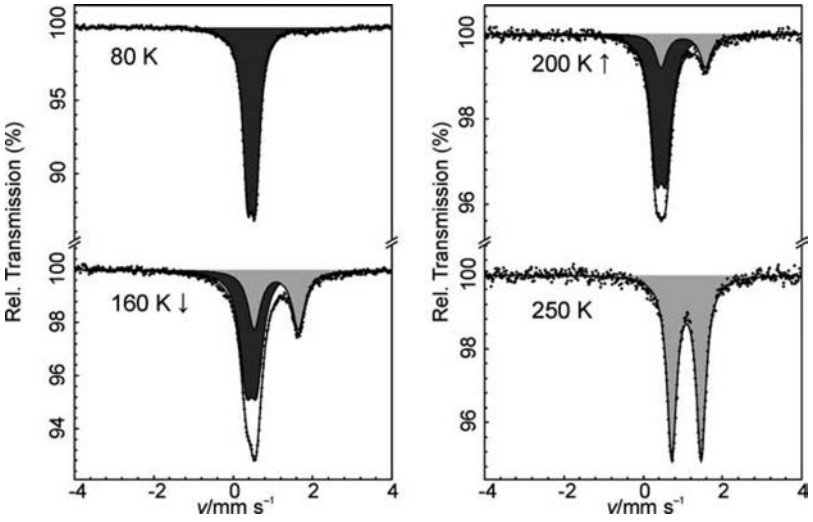

Figure 9. Mössbauer spectra of **1** at different temperatures. Light gray doublet corresponds to the HS fraction, dark gray to the LS fraction.

Table 3. Least-Squares-Fitted Mössbauer Data for Compounds **1**−**5**[a]

compound	T/K	spin state	δ/mm s^{-1}	ΔE_Q/ mm s^{-1}	$\Gamma_{1/2}$/ mm s^{-1}	A/%
1	80	LS	0.46(0)	0.20(0)	0.14(0)	100
	160 ↓	LS	0.46(0)	0.27(0)	0.19(0)	61.7(10)
		HS	1.09(1)	1.12(1)	0.19(0)	38.3(12)
	200 ↑	LS	0.45(0)	0.25(0)	0.17(0)	77.7(16)
		HS	1.00(1)	1.12(2)	0.17(2)	22.3(21)
	250	HS	1.09(0)	0.74(1)	0.15(0)	100
2	80	LS	0.46(0)	0.24(1)	0.18(0)	85.6(15)
		HS	1.25(2)	1.50(4)	*0.18*	14.4(15)
	130 ↓	LS	0.40(1)	0.16(3)	0.19(1)	31.7(15)
		HS	1.17(0)	1.26(1)	0.18(0)	68.3(17)
	130 ↑	LS	0.44(1)	0.22(1)	0.18(0)	76.4(8)
		HS	1.19(2)	1.25(4)	*0.18*	23.6(8)
	200	HS	1.12(0)	1.13(1)	0.16(0)	100
3	80	LS	0.46(0)	0.21(0)	0.14(0)	100
	250	HS	1.08(0)	0.71(1)	0.16(1)	100
4	80	LS	0.46(0)	0.22(0)	0.16(0)	100
	215	LS	0.43(10)	0.28(22)	0.21(2)	81.2(51)
		HS	1.12(41)	1.12(82)	*0.2*	18.8(44)
	250	LS	0.39(1)	0.68(2)	*0.2*	73.6(40)
		HS	0.99(3)	1.03(2)	*0.2*	26.4(45)
5	80	LS	0.45(0)	0.27(0)	0.18(0)	87.1(15)
		HS	1.36(2)	1.91(5)	*0.18*	12.9(15)
	300	LS	*0.4*	0.68(2)	0.24(2)	60.6(38)
		HS	1.03(1)	1.02(3)	*0.22*	39.4(29)

[a] The values given in italics were fixed during fitting.

intermediate region, both doublets coexist. The HS/LS ratios are in complete agreement with the presence of magnetic hysteresis. Similarly, the Mössbauer spectra of **2** show a dependence on temperature and on the mode of the measurements. However, even at 80 K, a HS doublet is observed, which confirms the incompleteness of the transition. Values of the Mössbauer parameters from a least-squares fit are listed in Table 3. The variation of the molar HS fraction, γ_{HS}, compares well with those deduced from the magnetic susceptibility measurements, as indicated in Figure 8a−c for compounds **1**−**3**, respectively.

Despite the magnetic data confirming the completeness of the spin transition in **4** and **5**, the Mössbauer spectrum at high temperatures cannot be satisfactorily fitted by LS and HS doublets (see Figure 10). The spectrum is broadened, which is indicative of spin conversion rates

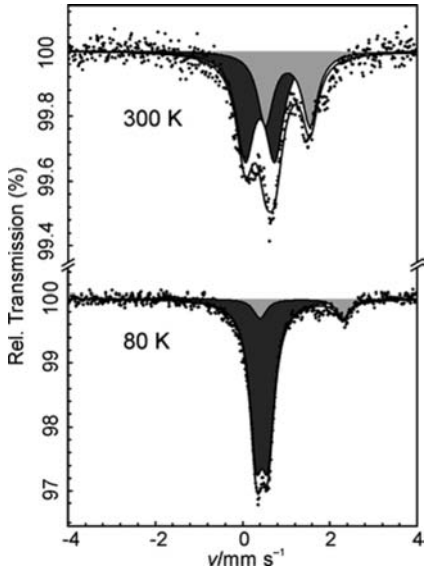

Figure 10. Mössbauer spectrum of **4** at indicated temperatures and fits. Light gray doublet corresponds to the HS fraction, dark gray to the LS fraction.

comparable to the hyperfine frequencies ($\sim 10^8$ s^{-1}).[53,54] This behavior was observed by Agustí et al. in a 3D Fe(II) Hofmann-like polymer, where line broadening of the resonance doublets is typical of a rapid interconversion of spin states.[33]

Differential Scanning Calorimetry (DSC) and Thermogravimetric Analysis. The differential scanning calorimetric measurements have been carried out in the 175−300 K temperature range at a rate of 7 K min^{-1} on the pristine samples. The temperature dependence of the heat flow in the heating and cooling modes for **1**−**3** is shown in Figure 11a−c. The features in the heat flow for **1** appear in the cooling mode at $T_c^{\downarrow} = 169$ K and $T_c^{\uparrow} = 199$ K in the warming mode, thus indicating the occurrence of a hysteresis with a width of 30 K. These values agree reasonably well with those observed from the $\chi_M T$ versus

(53) Adler, P.; Spiering, H.; Gütlich, P. *J. Phys. Chem. Solids* **1989**, *50*, 587–597.
(54) Adler, P.; Hauser, A.; Vef, A.; Spiering, H.; Gütlich, P. *Hyperfine Interact.* **1989**, *47*−*48*, 343–356.

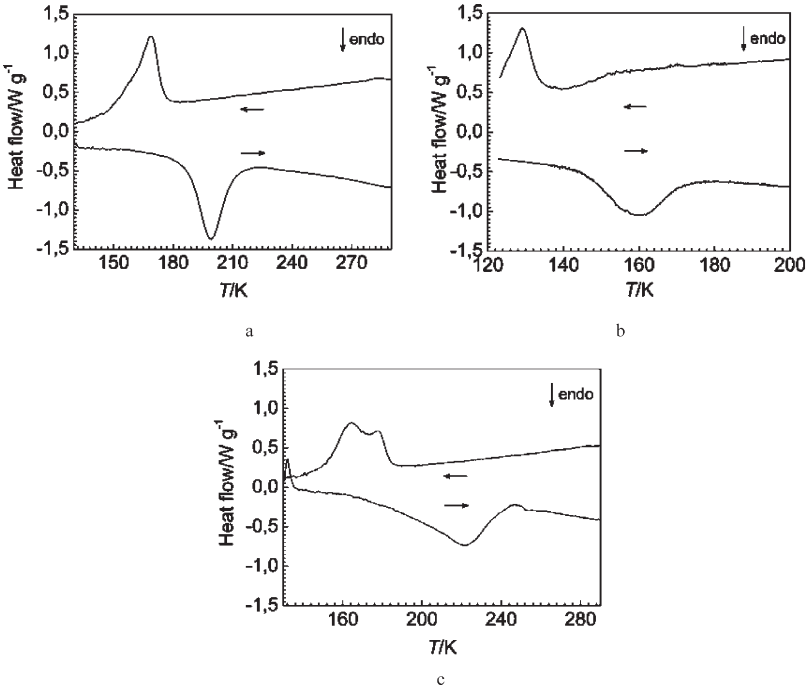

Figure 11. Differential scanning calorimetry curves for **1** (a), **2** (b), and **3** (c). The run directions are shown by arrows.

T plot. Similarly, compound **2** exhibits anomalies in the heat flow at $T_c^{\downarrow} = 129$ K and $T_c^{\uparrow} = 160$ K and **3** at $T_c^{\downarrow} = 170$ K and $T_c^{\uparrow} = 221$ K, which also match reasonably well with the magnetic data. The small differences in critical temperatures between the DSC and magnetic data are due to the different heating and cooling rates used in the experiments. Table 4 summarizes the derived thermodynamic parameters ΔH_{SCO} and ΔS_{SCO} for **1**−**3**; the ΔS values deduced from the DSC curves are somewhat larger than usually observed for most iron(II) spin-crossover compounds but compare well with those reported for {Fe(L)-[M^{II}(CN)$_4$]} (M^{II} = Ni, Pd, Pt) (L = pyridine,[20] pyrazine[29]), in line with the strong cooperative nature of the transitions.

Thermogravimetric measurements performed on **1**−**5** show that compounds **1** and **2** are anhydrous, whereas **3** and **4** contain about one molecule of water and **5** about one-half molecule of water per polymeric unit (the Supporting Information, SFigure 3). These results contribute to an explanation of the influence of the heating up to 400 K on the magnetic properties.

Discussion

One of the main goals of our research during the past few years has been the exploration of multifunctional materials combining spin crossover with another property which can interplay or interact in a synergic fashion with the spin-crossover phenomenon. In pursuing this research line, we have investigated parent SCO systems which can be chemically modified to introduce liquid crystalline functionality[55−57] leading to SCO metallomesogens.[41−44] Further development of this topic points to the Fe(II) two-dimensional polymers, among which the best candidate systems are the cyanide-bridged two-dimensional polymers of Fe(II). Many of them show cooperative spin transition at relatively high temperatures and a priori seem to be suitable for chemical modification in order to introduce the liquid-crystal properties. Indeed, the layered structure of the polymers allows chemical functionalizing of the ligands while retaining the polymeric organization of the cyanide networks and the N_6 environment of the iron(II) ions. For this reason, we have selected as parent systems Fe(II) polymers based on 4-phenylpyridine, which are perfectly suited for the grafting of alkyl chains. The modification of the ligand 4PhPy incorporating the liquid-crystal moieties is depicted in Figure 12.[58]

Table 4. Thermodynamic Parameters for Compounds **1**−**3** Derived from the DSC Data

	ΔH_{SCO}/kJ mol^{-1}	ΔS_{SCO}/J mol^{-1} K^{-1}
1	11.8	64.1
2	7.8	55.7
3	12.8	64.0

As we could not obtain good-quality crystals of **1**−**5**, the first goal was to perform structural characterization of the compounds using powder X-ray diffraction measurements. The proposed atomic distribution in **1**−**5** is based on the spectroscopic (Mössbauer, EXAFS, EDXA, and IR), magnetic, and TGA data and chemical arguments.

The EXAFS data of compounds **1** and **2** match reasonably the atomic distribution of the analogous compound {Fe(py)$_2$[Ni(CN)$_4$]} characterized structurally by single-crystal X-ray diffraction.[16] In contrast with the magnetic data, XAS analysis reveal more gradual and incomplete spin transition for studied samples **1** and **2**. As already discussed in the literature,[59]

(55) Seredyuk, M.; Gaspar, A. B.; Kusz, J.; Bednarek, G.; Gütlich, P. *J. Appl. Crystallogr.* **2007**, *40*, 1135–1145.
(56) Seredyuk, M.; Gaspar, A. B.; Munoz, M. C.; Verdaguer, M.; Villain, F.; Gütlich, P. *Eur. J. Inorg. Chem.* **2007**, 4481–4491.
(57) Seredyuk, M. Ph.D. Thesis, University of Mainz, Mainz, Germany, 2008.
(58) Manuscript in preparation.
(59) Boca, R.; Vrbova, M.; Werner, R.; Haase, W. *Chem. Phys. Lett.* **2000**, *328*, 188–196.

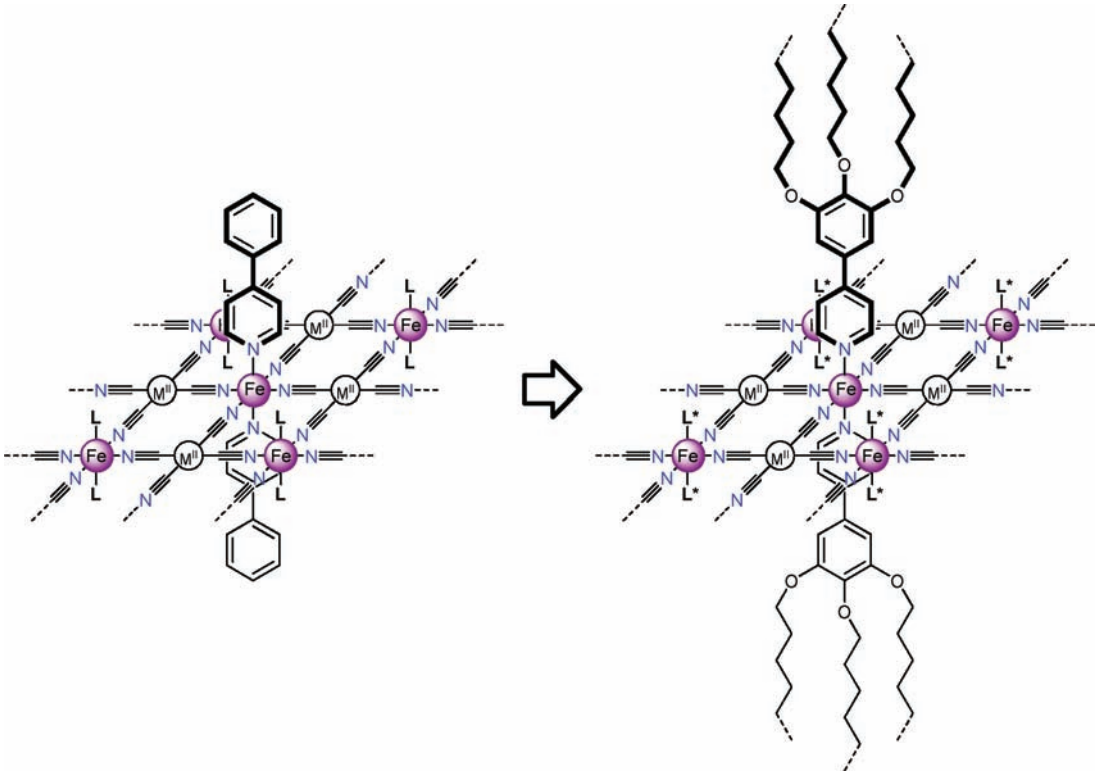

Figure 12. Example of modification of the Hoffman-like system $\{Fe(4PhPy)_2[M^{II}(CN)_4]\}$ by introduction of alkoxy substituents to phenyl moieties of the ligands. L is 4PhPy, L* is 4-(3,4,5-trisalkoxyphenyl)pyridine.

the XAS data of spin-crossover compounds are very sensitive to (i) grinding of the samples, (ii) pelletization under pressure, and (iii) possible differences between the real temperature of the sample and that of the temperature sensor situated outside the sample. In the case of mechanically unperturbed samples, the variable-temperature magnetic and Mössbauer data, and, on the other hand, structural PXRD characterization, give practically similar results with a somewhat broader hysteresis loop in the case of structural data, which can be attributed to different heating and cooling rates in different techniques.

Among the reported 2D Fe(II) polymers,[16−38] polymers **1**−**3** exhibit the strongest cooperative spin transition with thermal hysteresis cycles of 20−40 K width. The relatively large entropy gain upon SCO in **1**−**3** (∼65 J K^{-1} mol^{-1}) reflects the strong cooperativity of these spin transitions. Although we could not analyze the crystal packing of the compounds, it is reasonable to assume in analogy with related systems[16,20] that the origin of the cooperativity is connected with the intralayer interactions between the Fe(II) centers through the CN bridging ligands. Short contacts between phenyl rings of adjacent layers that transmit the structural modification of the Fe(II) core through the whole solid could also play a role.

Entropy, ΔS, has two components, one of electronic origin associated essentially with the difference of spin multiplicity of the involved LS and HS states [$\Delta S^{el} = k_B \ln[(2S^{HS} + 1)/(2S^{LS} + 1)] = 13.45$ J K^{-1} mol^{-1} for a Fe(II) SCO system], the other component reflecting the different density of vibrational states, $\Delta S^{vibr} = \Delta S - \Delta S^{el}$, mostly arising from the difference of Fe−N bond lengths (ca. 0.2 Å) between the two spin states. An estimation of the vibrational contribution to ΔS^{vibr} performed for pyridine and pz derivatives based on vibrational spectroscopy has shown that most low-frequency modes suffer dramatic changes upon spin transition. For example, the stretching modes of the $[FeN_6]$ core change by 160−180 cm^{-1}, a fact already noted for other iron(II) SCO compounds.[29,60] However, an important and genuine additional source of entropy is the stretching M−C and M−C−N bending modes of the $[M^{II}(CN)_4]^{2-}$ counterion. They experience shifts of ca. 40−70 cm^{-1} and 150 cm^{-1} due to HS-to-LS transition, respectively, indicating that these modes are strongly coupled with those of the $[FeN_6]$ core. This is a reasonable finding also for compounds **1**−**3** since, in such compounds, building blocks are covalently bonded, affording a robust $\{Fe[M^{II}(CN)_4]\}_\infty$ 2D framework, which enables long-range elastic interactions responsible, in part, for the cooperativity and hysteresis exhibited for these compounds. The difference in SCO behavior can be ascribed instead to the variation of the axial ligands. For example, in the pyridine series, the pyridine rings of consecutive interdigitated layers are defined infinite stacks characterized by an almost face-to-face superposition along the [010] direction.[16] The resulting $\pi-\pi$ interactions, although relatively weak (C···C distances ca. 3.75 Å), add an additional contribution to cooperativity. Consequently, the doubled $\pi-\pi$ interactions in **1**−**3** due to the ligand 4PhPy afford enhanced cooperativity, a wider hysteresis, and a larger contribution to ΔS^{vibr}.

The replacement of $[M^{II}CN)_4]^{2-}$ anions with $[M^{I}(CN)_2]^-$ (M = Ag, Au) groups results in another type of coordination in polymers **4** and **5** with decreased cooperativity of the spin transition. The transition occurs without thermal hysteresis, but relatively abruptly, especially for the dehydrated compounds. Chemical arguments, spectroscopic data, and the spin-crossover properties suggest that the

(60) Sorai, M.; Nakano, M.; Miyazaki, Y. *Chem. Rev.* **2006**, *106*, 976–1031.

structures of **4** and **5** are similar to those reported for $\{Fe(py)_2[Ag(CN)_2]_2\}$[32] and $\{Fe(py)_2[Au(CN)_2]_2\}$.[36]

Conclusion

A novel family of two-dimensional coordination polymers displaying thermally and light induced spin transition has been synthesized. Magnetic measurements indicate strongly cooperative spin transition with an hysteresis width up to ca. 40 K in $[M^{II}(CN)_4]$-based Fe(II) polymers. The hysteresis is modulated by solvent water molecules. The variable temperature PXRD technique reveals the occurrence of a first-order structural phase transition for compound **1**. In the derivatives of $[M^{I}(CN)_2]$ groups, the transition is less cooperative, without hysteresis, and is also solvent-dependent. All compounds are thermochromic. The characterization of the materials by various techniques indicates that their structure is layerlike with 2D polymeric entities similar to the pyridine analogues. These features appears suitable for the development of modified systems with liquid-crystalline properties.

Experimental Section

All reagents were purchased from Aldrich or Acros and used as received.

Synthesis of $[N(n\text{-}Bu)_4]_2[M^{II}(CN)_4]$ (M^{II} = Pd, Ni, Pt) and $[N(n\text{-}Bu)_4][M^{I}(CN)_2]$ (M^{I} = Ag, Au). A concentrated solution of $K_2[M^{II}(CN)_4]$ or $K[M^{I}(CN)_2]$ was treated with a 20% less than stoichiometric amount of $[N(n\text{-}Bu)_4]Br$. The resulting solution was extracted with an equal volume of chloroform. The organic phase was then evaporated to dryness, yielding a white powdery solid that was collected and dissolved in a small amount of chloroform. The solution was carefully filtered to remove all insoluble matter, and the filtrate was evaporated to dryness.

Anal. calcd for $[N(n\text{-}Bu)_4]_2[Pd(CN)_4]$, $C_{36}H_{72}N_6Pd$: C, 62.18; H, 10.44; N, 12.08. Found: C, 62.06; H, 10.35; N, 11.98. Anal. calcd for $[N(n\text{-}Bu)_4]_2[Ni(CN)_4]$, $C_{36}H_{72}N_6Ni$: C, 66.76; H, 11.20; N, 12.98. Found: C, 66.28; H, 10.67; N, 12.18. Anal. calcd for $[N(n\text{-}Bu)_4]_2[Pt(CN)_4]$, $C_{36}H_{72}N_6Pt$: C, 55.15; H, 9.26; N, 10.72. Found: C, 55.12; H, 9.15; N, 10.68. Anal. calcd for $[N(n\text{-}Bu)_4][Ag(CN)_2]$, $C_{18}H_{36}AgN_3$: C, 53.73; H, 9.02; N, 10.44. Found: C, 53.37; H, 9.83; N, 10.47. Anal. calcd for $[N(n\text{-}Bu)_4][Au(CN)_2]$, $C_{18}H_{36}AuN_3$: C, 43.99; H, 7.38; N, 8.55. Found: C, 43.32; H, 7.39; N, 8.45.

Synthesis of 1−5. The synthesis was performed under a nitrogen atmosphere. To a methanolic solution containing $Fe(BF_4)_2\cdot 6H_2O$ (0.1 g, 0.3 mmol, 10 mL) was added dropwise a solution of 4-phenylpyridine in MeOH (0.6 mmol, 10 mL). To the resulting orange solution was added 0.3 mmol of $[N(n\text{-}Bu)_4]_2[M^{II}(CN)_4]$ (M^{II} = Pd, Ni, Pt) or 0.6 mmol of $[N(n\text{-}Bu)_4][M^{I}(CN)_2]$ (M^{I} = Ag, Au) dissolved in 10 mL of methanol, leading to the formation of a yellow precipitate. The precipitate was filtered off and washed with MeOH and subsequently dried in a vacuum overnight. Anal. calcd for **1**, $C_{26}H_{18}FeN_6Pd$: C, 54.15; H, 3.15; N, 14.57. Found: C, 54.23; H, 3.15; N, 14.70. Anal. calcd for **2**, $C_{26}H_{18}FeN_6Ni$: C, 59.03; H, 3.43; N, 15.89. Found: C, 59.47; H, 3.41; N, 15.96. Anal. calcd for **3**, $C_{26}H_{20}FeN_6OPt$: C, 45.69; H, 2.95; N, 12.30. Found: C, 46.01; H, 2.77; N, 12.60. Anal. calcd for **4**, $C_{26}H_{20}Ag_2FeN_6O$: C, 44.35; H, 2.86; N, 11.94. Found: C, 44.28; H, 2.72; N, 12.04. Anal. calcd for **5**, $C_{26}H_{19}Au_2FeN_6O_{0.5}$: C, 35.76; H, 2.19; N, 9.62. Found: C, 36.06; H, 2.63; N, 9.70. EDXA (energy-dispersive X-ray microanalysis) found: **1**, (50%Fe/50%Pd); **2**, (50%Fe/50%Ni); **3**, (50%Fe/50%Pt); **4**, (33%Fe/67%Ag); **5**, (33%Fe/67%Au).

Instrumentation. X-Ray Absorption Data Recording and Processing. The iron *K*-edge X-ray absorption near-edge structures and EXAFS spectra were recorded in the conventional transmission mode on beamline A1 at the German Electron Synchrotron, DESY, Hamburg. The spectrum was recorded from 6970 to 7997 eV. The energy scale at the iron *K*-edge was calibrated with the strong absorption peak of metallic iron foil at 7111.2 eV. A water-cooled Si(111) channel-cut crystal was used as a monochromator. The intensities of the incident and transmitted X-rays were recorded using ionization chambers. The mass of the sample was calculated to obtain a product $a \times d$ of about 2.5 for energies just above the absorption *K*-edge of iron (a is the linear absorption coefficient, and d is the thickness of the pellet). The calculated amount of the sample was ground, mixed with crystalline cellulose, and pressed into a 13-mm-diameter and about 1-mm-thick pellet. A closed-cycle He cryostat was used for variable-temperature measurements. The temperature was measured with a Si diode placed close to the sample. The data acquisition time for each data point was 1 s. EXAFS data analysis was performed with the program EXAFS98.[61,62] This standard analysis includes linear pre-edge background removal, a Lengeler−Eisenberg spectrum normalization, and reduction from the absorption data $\mu(E)$ to the EXAFS spectrum $\chi(k)$ with

$$k = \sqrt{\frac{2m_\varepsilon}{(\hbar)^2}(E - E_0)}$$

where E_0 is the energy threshold, taken at the absorption maximum (7130 ± 1 eV). The radial distribution function $F(R)$ was calculated by the Fourier transformation of $k^3 w(k)\chi(k)$ in the 2−14 Å^{-1} range; $w(k)$ is a Kaiser−Bessel apodization window with smoothness coefficient $\tau = 3$. After Fourier filtering, the first single-shell Fe−N_6 was fitted in the 4−12 Å^{-1} range to the standard EXAFS formula, in a single scattering scheme:

$$k_\chi(k) = -S_0{}^2 \sum_{i=1.5} \left\{ \frac{N_i}{R_2^i} |(F\pi, k)| e^{-2\sigma^2 k^2} e^{-2R_i/\lambda(k)} \sin[2kR_i + 2\partial_1(k) + \psi(k)] \right\}$$

where $S_0{}^2$ is the inelastic reduction factor, N is the number of nitrogen atoms at a distance R from the iron center, $\lambda(k)$ is the mean free path of the photoelectron, σ is the Debye−Waller factor, giving the width of the Fe−N distance distribution, $\partial_1(k)$ is the central atom phase shift, and $|(F\pi,k)|$ and $\psi(k)$ are the amplitude and phase of the nitrogen backscattered wave. The curve-fitting analysis for the first coordination sphere of the iron was performed with the *Round Midnight*[63] code after Fourier filtering in the 0.7−2.0 Å range of the EXAFS spectrum. Spherical-wave theoretical amplitudes and phase shifts calculated by the *McKale*[64,65] code were used. Since theoretical phase shifts were used, we fitted the energy threshold E_0 (ΔE_0). The goodness of fit was given by

$$\rho(\%) = \frac{\sum[k\chi_{\exp}(k) - k\chi_{th}(k)]^2}{\sum[k\chi_{\exp}(k)]^2}$$

Variable-temperature magnetic susceptibility measurements of samples **1**−**5** (20−30 mg) were recorded with a Quantum Design MPMS2 SQUID susceptometer

(61) Michalowicz, A. EXAFS98 pour la Mac. In *Logiciels pour la Chimie*; Société Française de Chimie: Paris, 1991; p 102.
(62) Michalowicz, A. *J. Phys. IV France* **1997**, *7*, 235.
(63) Michalowicz, A. Round Midnight. In *Logiciels pour la Chimie*; Société Française de Chimie: Paris, 1991; p 116.
(64) McKale, A. G.; Knapp, G. S.; Chan, S. K. *Phys. Rev. B* **1986**, *33*, 841–846.
(65) McKale, A. G.; Veal, B. W.; Paulikas, A. P.; Chan, S.-K.; Knapp, G. S. *J. Am. Chem. Soc.* **1988**, *110*, 3763–3768.

equipped with a 7 T magnet, operating at 1 T and at temperatures from 1.8−400 K. The susceptometer was calibrated with $(NH_4)_2Mn(SO_4)_2 \cdot 12H_2O$. Experimental susceptibilities were corrected for diamagnetism of the constituent atoms by the use of Pascal's constants.

Mössbauer spectra were recorded in transmission geometry with a ^{57}Co/Rh source kept at room temperature and a conventional spectrometer operating in the constant-acceleration mode. The samples were sealed in a Plexiglas sample holder and mounted in a nitrogen-bath cryostat. The Recoil 1.03a Mössbauer Analysis Software (Dr. E. Lagarec; http://www.isapps.ca/recoil/) was used to fit the experimental spectra.

DSC measurements were performed on a Mettler model DSC 822e calibrated with metallic indium and zinc. DSC profiles were recorded at a rate of 10 K/min and analyzed with Netzsch Proteus software (NETZSCH-Geraetebau GMBH, http://www.e-thermal.com/proteus.htm). An overall accuracy of 0.2 K was estimated in the temperature control and 2% in the heat flow.

High-resolution powder diffraction patterns were collected in Debye−Scherrer mode on the high-resolution powder diffractometer at ID31 of the European Synchrotron Radiation Facility (ESRF, Grenoble) coupled with a liquid-nitrogen cryostat. The samples were sealed in lithium borate glass capillaries of diameter 0.5 mm (Hilgenberg glass no. 50) and rotated around θ in order to improve the spatial averaging. The exact wavelength and the zero point were determined from well-defined reflections of a silicon standard (λ = 0.29941892 ± 0.00009008 Å). At ID31, nine crystal analyzers [nine Ge (111) crystals separated by 2° intervals] with nine Na(Tl)I scintillation counters were used simultaneously. The incoming beam was monitored using an ion chamber for normalization purposes in order to take the decay of the primary beam into account.

IR spectra were recorded at 293 K using a Bruker Tensor 27 Spectrometer in the range of 400−4000 cm^{-1}.

Elemental analyses were done on a Vario EL Mikro Elementaranalysator.

TGA measurements were performed on a Mettler Toledo TGA/SDTA 851, in the 300−680 K temperature range in a nitrogen atmosphere at a rate of 10 K/min.

Microanalysis was done by using a PV 9760 EDAX Microanalysis with a PHILIPS XL 30 ESEM scanning electron microscope.

Acknowledgment. We acknowledge the financial help from the Deutsche Forschungsgemeinschaft (Priority Program 1137 "Molecular Magnetism") and the Fonds der Chemischen Industrie. A.B.G. thanks the Spanish MEC for a Ramon y Cajal research contract, for the project CTQ 2007-64727, and the Alexander von Humboldt Foundation for work-visiting fellowships. We also thank Ms. E. Muth and Ms. P. Räder of the Max-Planck-Institute for Polymer Research, Mainz, for their help in performing TGA and DSC measurements. We are grateful to Dr. R. Dinnebier and Dr. K. Sugimoto, Max-Planck-Institute for Solid State Research, Stuttgart, and Dr. I. Margiolaki for their help in performing high-resolution PXRD measurements at the European Synchrotron Radiation Facility. We also acknowledge the support of the responsible scientists Dr. E. Welter from HASYLab and Dr. H. Ehrenberg and Dominic Stürmer from TU Darmstadt during the EXAFS measurements at beamline A1 and A. Michalowicz for providing us with his XAS analysis package.[63]

Supporting Information Available: Filtered signals of the EXAFS peaks I, II, and III for **1** and **2**. Results of the analysis of the first coordination shell (I) of **1** and **2**. Powder diffraction pattern of **1** at 80 (LS state) and 290 K (HS state) and of **2**−**5** at 290 K. TGA profiles for **1**−**5**. This material is available free of charge via the Internet at http://pubs.acs.org.